OSCILLATING WINGS AND BODIES WITH FLEXURE IN SUPERSONIC FLOW - APPLICATIONS OF HARMONIC POTENTIAL PANEL METHOD

ICAS-86-2.9.4

D. D. Liu[+], Pablo Garcia-Fogeda[*] and P. C. Chen[**]
Mechanical and Aerospace Engineering
Arizona State University
Tempe, Arizona 85287

ABSTRACT

The development of the Harmonic Gradient Method (HGM) and the Harmonic Potential Panel (HPP) method for nonplanar wings and bodies in unsteady supersonic flow is presented. They are proved to be accurate and versatile tools for computations of unsteady aerodynamics. According to a consistent formulation, the bases of both methods are now unified. Owing to the Harmonic Potential model, optimal number of panels can be achieved without loss of the computational accuracy. And yet it is least affected by the given Mach number and reduced frequency. Moreover, these methods are completely general in terms of input oscillatory frequencies, mode shapes and body or planform geometries. To validate the HGM/HPP computer codes, various computed results are compared with all known cases. These results demonstrate that the computer codes are attractive in their efficiency and cost-effectiveness for aeroelastic analyses, which suggest immediate industrial applications.

INTRODUCTION

With the advent of supersonic aircraft and modern launch vehicles, there exists a need for an accurate airload prediction method for aeroelastic design analysis. While current methodology for interfering lifting surfaces in the subsonic regime is better established due to the accomplishment of the Doublet Lattice Method (Ref. 1) an equally effective supersonic method has been lacking for several decades. Many attempts have been made in recent years for development of such an effective method in treatments of interfering configurations (e.g. Refs. 2-6). Most of the investigators followed Jones and Appa's Potential Gradient Method and modified it further. By contrast, the Harmonic Gradient Method (HGM, Ref. 5) developed in 1983 encompasses a generalized formulation for nonplanar lifting surfaces and with that it also achieves the requirements of computation accuracy and cost effectiveness. Among these attempts, the HGM appears to be one of the most promising methods to date. In fact, since 1983 several aircraft industries have already adopted the HGM for supersonic aeroelastic applications. To continue the development of the HGM, our current efforts have been engaged in the generalization of this method for axisymmetric bodies with flexture (Refs. 7-8), with a view towards a comprehensive program for computations of body-wing aerodynamics. In this paper developments of the HGM and the Harmonic Potential Panel (HPP) method in the problem areas for wings and bodies will be addressed.

The essence of the HGM, and now the HPP method, lies in the introduction of the Harmonic Potential (HP) model. With this model, substantial savings in the wing panel numbers can be achieved and yet without the loss of computation accuracy. Furthermore, both HGM and the HPP codes are completely general in terms of the input wing/body geometry, mode-shapes and reduced frequencies. The ease of application of these codes are comparable to that of the Doublet Lattice Code and the USSAERO Code (Ref. 9). With these features, both codes once combined can be attractive in that they can perform cost-effective analyses for complex aircraft configurations.

Meanwhile, the confidence level of these program codes depends largely on the result validation. For this reason, various computed results of wings and bodies will be presented for verification with all known cases.

GENERAL FORMULATION

Let $\sigma = 0$ represent the wing formulation and $\sigma = 1$ the body. The perturbed potential integral can be written in general as

$$\phi_\sigma(x_0, y_0, z_0) = I_\sigma\left[F_\sigma \left(\frac{\partial}{\partial n}\right)^\sigma H\right] \tag{1}$$

where $I_0[\ ] = \iint [\ ]dx\,dy$ and $I_1[\ ] = \int [\ ]dx$, F_0 and F_1 are the doublet strengths for the wing and the body, respectively. The kernel function reads

$$H(x-x_0,\ y-y_0,\ z_0) = \frac{\cos\frac{\mu R}{M_\infty}}{R} e^{-i\mu(x-x_0)} \tag{2}$$

where $\mu = kM_\infty^2/\beta^2$, M_∞ is the freestream Mach number and k is the reduced frequency.

On the surfaces of the wing and along the body axis, the doublet strengths of each panel can be expressed in terms of $a_{\sigma i}$ which can be obtained by solving the flow tangency equation on the panel surfaces,

$$\left[A_{\sigma ij}\right]\left\{a_{\sigma i}\right\} = \left\{\frac{Dh_{\sigma j}}{Dt}\right\} \tag{3}$$

where $A_{\sigma ij}$ represents the aerodynamic influence coefficient of the jth panel to the ith control point. $\frac{Dh_{\sigma j}}{Dt}$ represents the downwash, in which $h_{\sigma j}$ is the displacement of the jth panel.

The unsteady pressure coefficients are

$$c_p^\sigma = -2\left[\frac{\partial}{\partial x_0} + ik\right]\phi_\sigma(x_0, y_0, z_0)\, e^{ikt} \tag{4a}$$

for the wing ($\sigma = 0$), and

[+] Associate Professor, Member AIAA
[*] Graduate Assistant
[**] Graduate Student, Member AIAA

$$c_p^{\sigma} = c_{p_0} + \delta_0(\Delta c_p)\cos\theta\, e^{ikt} \qquad (4b)$$

for the body ($\sigma = 1$), where c_{p_0} is the mean-flow pressure and Δc_p represents the unsteady pressure due to a small amplitude δ_0. It should be noted that $a_{\sigma i}$ for the body depends on the mean-flow solution due to the nonvanishing of the body thickness. Consequently, Δc_p should also depend on the mean-flow pressure c_{p_0}. Since the wing thickness is approximated by a lifting surface, the $a_{\sigma i}$ and the unsteady pressure c_p^{σ} in Eqs (3) and (4a) are decoupled from the mean-flow solution.

STEADY-FLOW RESULTS

Swept Rectangular Wing

With the subsonic leading and trailing edges, the planform in Figure 1 is an interesting case for result verifications. An exact solution obtained by Cohen (Ref. 10) clearly indicates the wave-wave interaction feature of the problem (Figure 2). Among others, previous attempts by Chipman (Ref. 11) using improved Mach Box method and by Ueda and Dowell (Ref. 4) using Doublet Point method have shown smearing of data around wave-wave finite discontinuities. To capture these discontinuities, it is essential to create irregular panels along the Mach wave cuts. One type of the panel arrangements used by HGM code is shown in Figure 1b. With 196 panels, lifting pressures are computed at the spanwise locations of 48% and 72% as shown in Figures 2a and 2b. In so doing, both weak and strong wave discontinuities are properly captured in regions inboard and outboard of the tip Mach line, as well prescribed by Cohen's exact results.

Nonlinear Solutions for Bodies

Results of linear and nonlinear versions of HPP Code are presented in Figures 3 and 4. Based on Van Dyke's iterative procedure, the HPP nonlinear code has been developed recently (Ref. 8) to account for the nonlinear body thickness effects. It is the first time that the panel method, using the technique of particular solutions, is employed to tackle the nonlinear problem without involving the field point computations. In Figure 3, HPP results (linear) and HPP nonlinear results are compared with those computed by USSAERO Code and by exact characteristics for a 26% thick ogive body at $M_\infty = 2.0$ and 3.0. The HPP nonlinear results compare very well with those computed by the method of exact characteristics. It is seen that the nonlinear effect due to thickness is substantial from apex to the mid body. Next, the nonlinear iterative scheme is applied to a 16% thick ogive-cylinder-boattail body at $M_\infty = 3.0$ and placed at moderated angles of attack ($\alpha_0 = 3.2°$ and $6.3°$). Again, very good correlations are found with the computed results of the Parabolized Navier-Stokes (PNS) Code and the Euler Code (Ref. 12) for both cases in Figures 4a and 4b. Considerable deviations between the linear and the nonlinear results are again observed particularly on the windward side of the ogive part. It is believed that as long as the flow remains attached, the present HPP nonlinear method should expect to yield results in favorable agreement with those by computational methods in the supersonic Mach number range.

STABILITY DERIVATIVES

45° Delta Wing

For the panel arrangement as shown in Figure 5, the large aspect ratio of each panel element in the proximity of wing tips of a 45° swept delta wing would have ordinarily caused numerical errors. To show that such is not the case for the HGM, we compare present HGM results with Miles' exact solution in terms of damping-in-pitch lift and moment coefficients. It is seen that all are in very good agreement with the exact results. This implies that the HGM scheme used is a robust one in that the computed result is unaffected by the assigned panel shapes and sizes.

Cone-Frustrum Body

Damping-in-pitch moment cofficients for a cone-frustrum body are presented in Figure 6. Throughout the supersonic range, present HPP results are in excellent agreement with Platzer's linearized method of characteristics (Ref. 13) Close agreements are also found with Tobak and Wehrend's cone theory and with various measured data (Ref. 14).

Ogive-Cylinder Body

It can be seen that in Figure 7 the damping-in-pitch moments as computed by the present HPP methods are in fair agreement with the measured data for a 20% thick ogive-cylinder body throughout the Mach range. The computed results of SPINNER Code and that of Ericsson's (Ref. 27) show large discrepancies with measured data whereas little dependency was found in the Mach number range. By contrast, strong Mach number dependency is shown in the results of the HPP Code. However, no appreciable difference is found between the HPP linear and nonlinear resutls for this case.

HARMONIC POTENTIAL MODEL

To achieve computation accuracy and effectiveness for wings or bodies in high-frequency oscillations, it is essential to render the doublet solution and its convective gradient uniformly valid throughout the frequency domain. This is to say that the doublet strength in each panel can be maintained spatially harmonic. In so doing, the element size is made automatically compatible to the wave number generated along the chord. Hence, the solution obtained can be least affected by the panel length and the input frequency.

In terms of Eq (3), the HP model amounts to representing the unknown strengths $a_{\sigma i}$ by

$$a_{\sigma i} = (b_i + c_i x)e^{i\mu x} \qquad (5)$$

Figure 8 shows that the doublet potential $\Delta\phi$ (or F_0 and F_1) behaves according to Eq (5). As a result, as few as 30 panels are needed for a single wing planform using regular paneling scheme and 20 panels for a single body in actual computation (see Refs. 5 and 7). In an IBM 3081 computer, typically only 90 CPU seconds and 7 CPU seconds are required respectively for computations of unsteady pressures.

FULL-FREQUENCY DOMAIN

With the HP model built in, the HGM and the HPP methods can handle oscillatory problems in the full frquency domain effectively. In the high-frequency range, accurate solutions can be obtained without increasing the number of panel elements. Figures 9 and 10 present the unsteady pressures at the root chord section of a high-aspect-ratio rectangular wing in pitching and in plunging motions, respectively. For verification, the reduced frequencies k selected lie in the moderate to high range between 0.4 and 2.0 and the Mach numbers (M_∞ = 1.15 and 1.25) are selected in the lower range. As the root-chord is not contaminated by the tip Mach cone, it can be seen that the HGM results are in good agreement with several available two dimensional results of Chadwick-Platzer (Ref. 15) and of Liu and Pi (Ref. 16) in Figure 9 and with that of Jordan (Ref. 17) in Figure 10. For oscillating bodies, Figure 11 presents results in the high frequency limit. To validate the high-frequency solution of HPP Code, its computed results using 20 the panel elements are checked against results calculated based on the piston theory for a very slender parabolic ogive. The thickness ratio τ = 0.02 is selected according to the requirment of $\tau M_\infty k \ll 1$ as imposed by the piston theory. At M_∞ = 1.5, it is seen that the agreement seems to be very good for two selected frequencies k = 4.0 and k = 7.5. It is also interesting to compare the effects of frequency and flow dimensionality on unsteady pressures. Figure 12 shows comparisons of unsteady pressure coefficients for a 5.7° cone and a flat plate pitching about the apex at M_∞ = 2.0. The HPP results are compared with the LPP results (Ref. 16) which are identical with the HGM results for a rectangular wing at the root chord. As expected, the unsteady pressure magnitudes for an oscillating cone is smaller than those of a flat plate at k = 1.0 and k = 2.0. Similar to the case in steady supersonic cone and wedge flows, the present finding shows that the cone in oscillation yields weaker compressions as a result of three dimensionality of the flow, irrespective of the oscillation frequency.

OSCILLATING FLEXIBLE BODIES

Coordinate Systems

It has been observed that a slender missile is susceptible to flutter when it is under a combination of short-period rigid mode and free-free bending mode oscillation during its supersonic flight phase (Ref. 18). To analyze such problems requires the proper selection of the coordinate systems. This question has been studied in depth by Garcia-Fogeda and Liu (Ref. 7). Basically, there are three coordinate systems to be considered: the wind-fixed, the body-fixed, and the pseudo wind-fixed (see Figure 13). The first two systems have been subject to some controversy in the past (e.g. Refs. 19-22). We found that, if ill formulated, the wind-fixed system will yield solutions which are generally singular at the body apex and at the body slope discontinuities. On the other hand, based on Van Dyke's first order theory, a generalization of the body-fixed system can be readily formulated to facilitate present studies. The pseudo wind-fixed coordinate system is a hybrid approximation between the first two systems. Its formulation is physically correct but rigorous. It will be seen that the latter two systems yield similar trends for almost all cases.

Bending Oscillations

In Figure 14 the in-phase and out-of-phase pressures for a 10% thick ogive and cone-cylinder bodies with free-free first bending mode are presented. At Mach number M_∞ = 2.5 and reduced frequency k = 1.0, these results are computed in the body-fixed coordinate system. The presence of the pressure jumps, for the cone-cylinder case, obviously results from the flow turning corner at the shoulder. Next, in Figures 15 and 16, generalized aerodynamic forces of these bodies in first bending mode at k = 2.0 are evaluated in the range of supersonic Mach numbers. While the psuedo-wind-fixed and the body-fixed results are in satisfactory agreement, their deviations increase with increasing Mach number and thickness. Finally, in Figure 17, computed HPP results for an elastic cone-cylinder body were compared with the aerodynamic damping data measured by Hanson and Doggett (Ref. 23) for verification. The damping reduced frequency lies between 1.12 to 1.6, corresponding to M_∞ = 3.0 to 1.5. It is seen that the present results establish close trends to the measured data. By contrast, all quasi-steady theories yield much inferior predictions. It should be mentioned that equally close trends to the measured data were also predicted for the case of second order bending mode oscillations.

DIVERGENCE AND FLUTTER

The main application of the HGM and the HPP Codes lies in aeroelastic analyses such as the predictions of divergence and flutter boundaries. To verify these boundaries with measured data for wing planforms is difficult, as the latter are mostly kept out of the public domain. However, it should be noted that presently the HGM Code is used by several aircraft industries for flutter clearance purposes as well as flutter predictions in their aeroelastic optimization program. Also, limited amount of flutter data is found to exist for bodies.

In Figures 18, 19 and 20, an oscillating cone in rigid mode at wind-off frequency ratio of ω_H/ω_α = 1.8 is studied for divergence and flutter. The present HPP (linear) method and the HPP nonlinear method are used to compute the divergence and flutter boundaries. Here, the HPP nonlinear code is referred to a scheme using the nonlinear mean-flow solutions for unsteady-flow computations (see Ref. 8). It is seen that consistent improvement in trends are obtained for the nonlinear results over the linear ones in comparison with the measured data of Sewall, Hess and Watkins (Ref. 24). However, the predicted boundaries become less conservative in the order of slender-body, the HPP-linear and the HPP-nonlinear results. Almost no Mach-number dependency is shown for the divergence boundary as predicted by the HPP nonlinear code up to M_∞ = 5.0. In Figures 19 and 20 it is seen that overall trends of the predicted flutter speeds and frequencies are comparable to those measured. Since the cone is a slender one (cone semi angle = 7.5°), the predicted flutter speeds by the linear and the nonlinear methods merge in the low Mach number range as expected. A similar trend can be observed in the pressure distributions for the

mean-flow cases (see Ref. 25). It should be noted that for thicker bodies, the linear and the nonlinear results are expected to deviate from each other, as indicated by Van Dyke for the mean-flow cases.

OTHER CONFIGURATIONS

Saturn Launch Vehicle

In Figure 21, aerodynamic damping of the Saturn SA-1 launch vehicle is presented. To compare with Hanson and Doggett's measured data (Ref. 26), the free-free first bending mode and damping frequencies as determined by the experiment are used as the inputs for the present HPP Code. The natural frequency for the actual vehicle is 2.8 Hz, however, for wind tunnel experiments, the model natural frequency is 153 Hz due to the necessary scale-down in size. Consequently, the reduced frequency lies between 1.4 to 2.53 for Mach number range between 3.0 to 1.2 respectively. Thus, the reduced frequency range for the model study is of order unity. This then justifies the necessity of a general method such as the present HPP method which is valid in the full frequency domain. Good agreements are seen between present results and the measured data. To model this complex configuration, less than 100 panels are used with the given frequency range. Only 30 seconds CPU time on an IBM 3081 computer were needed for computing the aerodynamic damping coefficient for one freestream Mach number.

Northrop F-5 Wing

Tijdeman et al at NLR have performed a series of experiments on a pitching F-5 wing throughout the whole transonic range (Ref. 28). We select the highest Mach number case in this series (M_∞ = 1.336) for the computation example. With the pitching axis located at 50% of the root chord, the wing is pitching at a frequency of k = 0.198. Sections 1, 3 and 7 are selected which are located at 18%, 51.2% and 87.5% of the semi-span.

The HGM Code computes this case without the scheme of the Mach wave cut. It is seen that the correlations between the computed results and the measured data are fair. The reason for this is that physically there exists strong influence of the nonlinear effect due to a detached shock wave near the leading edge, whereas the HGM is a linear method. Also observed is the oscillatory feature of the measured data. This can be explained by the mentioned nonlinear effect in that the upstream-propagated unsteady waves are interacting with the detached shock wave which reflect upon the wing surface. We believe that the oscillatory pressures in this flow regime could in turn affect the flutter results to a certain extent. Investigation of this problem requires the careful study of the nonlinear transonic/supersonic flow at the near shock-attachment or detachment conditions. Such a study is in progress at ASU.

Nonplanar Wings

Computations were carried out for a wing and a tailplane, both with delta planforms in tandem configuration, as shown in Figure 23. Two coplanar cases and three nonplanar cases are considered according to Woodcock and York (Ref. 29). The fixed geometric parameters for this arrangement are,

root chords: OB = $2\sqrt{3}$ and PF = $\sqrt{3}/2$
wing spans: AC = 4 and EG = 2,

whereas the varied parameters are 'd', the distance between the wing and the tail measured along the x-axis from one trailing edge to the other, and 'h', the height between the mean planes of the wing and the tail. Case 2 and Case 5 are two special cases. In Case 2, the co-planed wing and tail join at point B (also now point P), in Case 5, no interference occurs between the two surfaces.

Four modes were considered,

mode 1: both wing and tail in plunging motion
mode 2: both wing and tail in pitching motion
mode 3: the tail alone in plunging motion
mode 4: the tail alone in pitching motion,

while the pitch axis remains fixed at 2/3 of the wing root chord for all modes.

The generalized forces should read,

$$\rho_\infty U_\infty^2 L^2 S(Q'_{IJ} + ik\, Q''_{IJ})$$

where 'L' is the reference chord length, 'S' is the reference span length and 'k' the reduced frequency, and they are set to $\sqrt{3}$, 2 and 0.01, respectively, for the present cases.

Only the out-of-phase part of the generalized forces, Q''_{IJ}, is presented in Tables 1 and 2. Computed results of HGM are compared with those by Woodcock and York using the Box Collocation method and by an approximate method of Martin et al (Ref. 30). Close agreement with Woodcock's results are found for the coplanar cases. For the nonplanar cases, some deviations are found in the values of Q''_{12}, Q''_{21}, Q''_{31}, and Q''_{41}.

It should be noted that the present HGM adopts a total of 125 panels, 100 for the wing and 25 for the tail, whereas Woodcock uses 350 boxes. In our earlier work (Ref. 5), as few as 50 panels were used to compute for an AGARD Wing-Tail-Fin combination. Practically little difference was found in the generalized forces between using 100 panels and 50 panels to represent the cases of wing-tail and fin-tail interferences.

CONCLUDING REMARKS

It has been shown that the present method has the following advantage over the existing unsteady supersonic methods:

1) The present method is formulated consistently based on the Harmonic Potential Model. It is general in the frequency domain and for arbitrary input mode shapes.

2) The present method is general for computing nonplanar or coplanar wing planforms as well as for axisymmetric bodies with any given body shape including slope discontinuities.

3) Due to the Harmonic Potential Model, the required number of panels is least affected

by the given Mach number and reduced frequencies, and yet without the loss of computational accuracy.

4) Both HGM and HPP Codes are computationally efficient in terms of computing time. The ease of application of these codes is comparable to that of the subsonic Doublet Lattice Code.

Therefore we believe that a comprehensive three-dimensional, unsteady supersonic method for body-wing combinations is nearly in hand. With the above features when both codes are properly combined in one, it can provide aircraft industries a cost-effective tool in performing supersonic aeroelastic analyses for a complex aircraft configuration. Presently we are continuing our effort towards this goal.

REFERENCES

1. Rodden, W.P., Giesing, J.P., and Kalman, T.P., ''New Developments and Applications of the Subsonic Doublet-Lattice Method for Non-planar Configurations,'' AGARD Symposium on Unsteady Aerodynamics for Aeroelastic Analyses of Interfering Surfaces, Paper No. 4, May, 1970.

2. Jones, W.P. and Appa, K., ''Unsteady Supersonic Aerodynamic Theory for Interfering Surfaces by the Method of Potential Gradient,'' NASA CR-2898, 1977.

3. Hounjet, M.H.L., ''An Improved Potential Gradient Method to Calculate Airloads on Oscillating Supersonic Interfering Surfaces,'' Journal of Aircraft, Vol. 19, No. 15, 1982, pp. 390-399.

4. Ueda, T. and Dowell, E.H., ''Doublet-Point Method for Supersonic Unsteady Lifting Surfaces,'' AIAA Journal, Vol. 22, No. 2, February 1984, pp. 179-186.

5. Chen, P.C., and Liu, D.D., ''A Harmonic Gradient Method for Unsteady Supersonic Flow Calculations,'' AIAA Paper 83-0887-CP, also Journal of Aircraft, Vol. 22, No. 5, May 1985, pp. 371-379.

6. Zhang, F.Q. and Forsching, H., ''An Improved Potential Gradient Method for the Calculation of Unsteady Aerodynamic Pressures on Oscillating Wings in Supersonic Flow,'' Paper No. 10, Second International Symposium on Aeroelasticity and Structural Dynamics, Aachen, W. Germany, April 1-3, 1985, pp. 153-1862.

7. Garcia-Fogeda, P. and Liu, D.D., ''A Harmonic Potential Panel Method for Flexible Bodies in Unsteady Supersonic Flow,'' AIAA Paper No. 86-007, 1986.

8. Garcia-Fogeda, P. and Liu, D.D., ''Aeroelastic Applications of Harmonic Potential Panel Method to Oscillating Flexible Bodies in Supersonic Flow,'' AIAA Paper No. 86-0864-CP, 1986.

9. Woodward, F.A., ''An Improved Method for the Aerodynamic Analysis of Wing-Body-Tail Configuration in Subsonic and Supersonic Flow,'' NASA CR-2228, 1973.

10. Cohen, D., ''Formulas for the Supersonic Loading, Lift and Drag of Flat Swept-Back Wings with Leading Edges Behind the Mach Line,'' NACA Report 1050.

11. Chipman, R., ''An Improved Mach-Box Approach for Supersonic Oscillatory Pressures,'' Journal of Aircraft, Vol. 14, Sept. 1977, pp. 887-893.

12. Schiff, L.B. and Sturek, W.B., ''Numerical Simulation of Steady Supersonic Flow Over an Ogive-Cylinger-Boattail Body,'' AIAA Paper No. 80-0066, 1980.

13. Platzer, M.F., and Sherer, A.D., ''Dynamic Stability Analysis of Bodies of Revolution in Supersonic Flow,'' Journal of Space and Rockets, Vol. 5, No. 7, July 1968, pp. 833-837.

14. Tobak, M. and Wehrend, W.R., ''Stability Derivatives of Cones at Supersonic Speeds,'' NACA-TN 3788, September, 1956.

15. Chadwick, W.R., ''Unsteady Supersonic Cascade Theory Including Nonlinear Thickness Effects,'' Ph.D. Thesis, Naval Postgraduate School, June 1975, also AGARD CP-177, September 1975.

16. Liu, D.D. and Pi, W.S., ''Transonic Kernel Function Method for Unsteady Flow Calculations Using a Unified Linear Pressure Panel Procedure,'' AIAA Paper No. 80-0737-CP.

17. Jordan, P.F., ''Aerodynamics Flutter Coefficients for Subsonic, Sonic and Supersonic Flow (Linear Two-Dimensional Theory),'' Aeronautical Research Council RM 2932, 1957.

18. Farrar, D.J., ''Structures,'' Journal of the Royal Aeronautical Society, Vol. 60, November 1956, pp. 712-720.

19. Hoffman, G. and Platzer, M.F., ''On Supersonic Flow Past Oscillating Bodies of Revolution,'' AIAA Journal, Vol. 4, 1966, p. 370.

20. Labrujere, Th.E., Roos, R., and Erkelens, L.J.J., ''The Use of Panel Methods with a View to Problems in Aircraft Dynamics,'' NLR MP-77009U.

21. Platzer, M.F. and Liu, D.D., ''A Linearized Characteristics Method for Supersonic Flow Past Bodies of Revolution Performing Bending Oscillations,'' Report LMSC/HREC A784262, Lockheed Missiles and Space Company, May 1967.

22. Hoffman, G.H. and Platzer, M.F., ''Higher Approximations for Supersonic Flow Past Slowly Oscillating Bodies of Revolution,'' Acta Mechanica, Vol. 5, 1968, pp. 143-162.

23. Hanson, P.W. and Doggett, R.V., ''Wind-Tunnel Measurements of Aerodynamic Damping Derivatives of a Launch Vehicle Vibrating in Free-Free Bending Modes at Mach Numbers from 0.70 to 2.87 and Comparisons with Theory,'' NASA TN D-1391, October 1962.

24. Sewall, J.L., Hess, R.W., and Watkins, C.E., ''Analytical and Experimental Investigation of Flutter and Divergence of Spring-Mounted Cone

Configurations at Supersonic Speeds,'' NASA TN D-1021, April 1962.

25. Van Dyke, M.D., ''First and Second Order Theory of Supersonic Flow Past Bodies of Revolution,'' Journal of Aeronautical Sciences, Vol. 18, No. 3, March 1951, pp. 161-178.

26. Hanson, P.W. and Doggett, R.V., ''Aerodynamic Damping of a 0.02-Scale Saturn SA-1 Model Vibrating in the First Free-Free Bending Mode,'' NASA TN D-1956, September 1963.

27. Ericsson, L.E., ''Viscous Effects on Missile Aerodynamics at Low Angles of Attack,'' J. Spacecraft and Rockets, Vol. 18, No. 5, September-October 1981, pp. 401-405.

28. Tijdeman et al, ''Transonic Wind Tunnel on an Oscillating Wing with External Store, part II: The Clean Wing,'' NLR TR 78106, part II, also AFFDL-TR-78-194, May 1982, pp. 20-1 to 20-25.

29. Woodcock, D.L. and York, E.J., ''A Supersonic Box Collocation Method for the Calculation of Unsteady Airforces of Tandem Surfaces,'' AGARD-CP-80-71 Symposium on Unsteady Aerodynamics for Aeroelastic Analysis of Interfering Surfaces, Part I, Paper No. 6.

30. Martin, J.C., Diederich, M.S., and Bobbit, P.J., ''A Theoretical Investigation of the Aerodynamids of Wing-Tail Combinations Performing Time-Dependent Motions at Supersonic Speeds,'' NACA TN 3072, 1954.

ACKNOWLEDGEMENT

The authors would like to thank Richard Chipman of Grumman Aerospace Corporation for valuable discussions and his suggestion of the swept-rectangular wing case. The present work is supported in part by the U.S. Army Research Office.

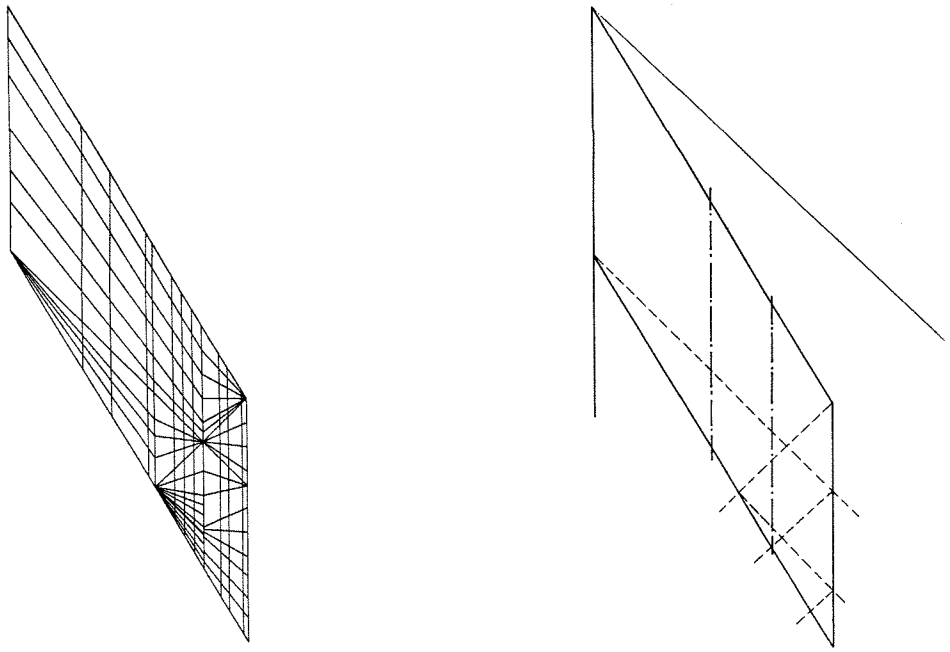

Fig. 1a, 1b Planform and Paneling Scheme for a Swept Rectangular Wing.

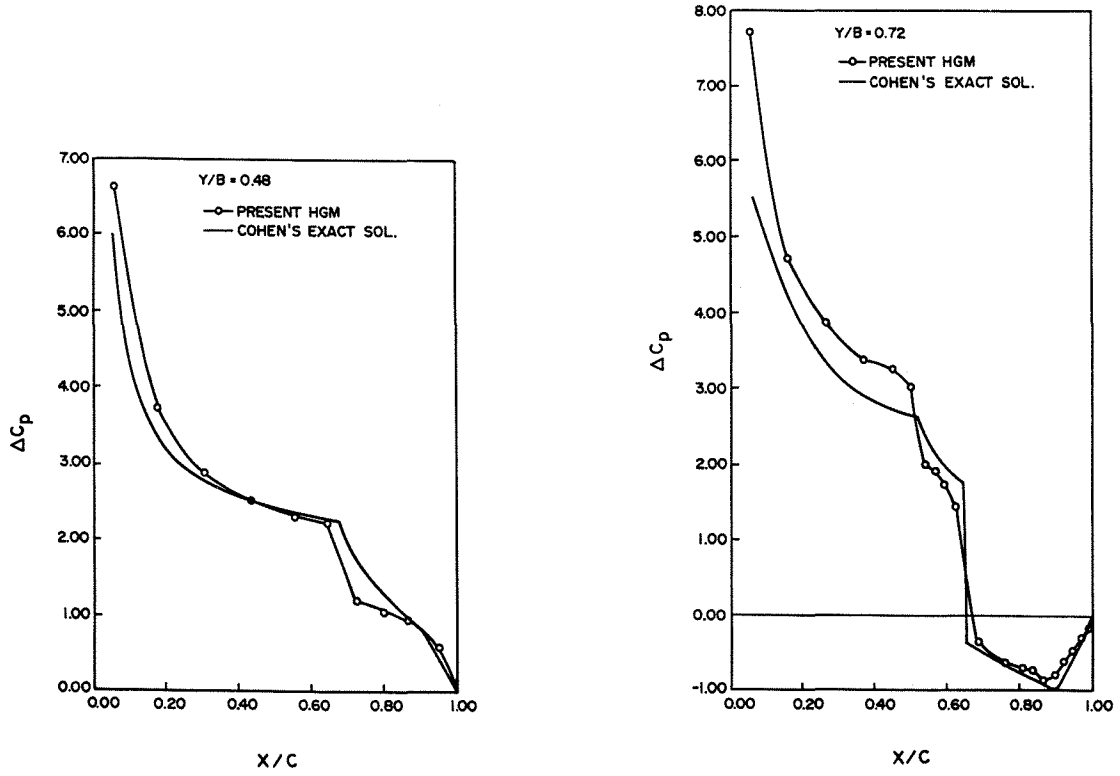

Fig. 2 Chordwise Steady Pressure Distribution for Swept Rectangular Wing at Angle of Attack. (a) Y/B = 48%, (b) Y/B = 72%

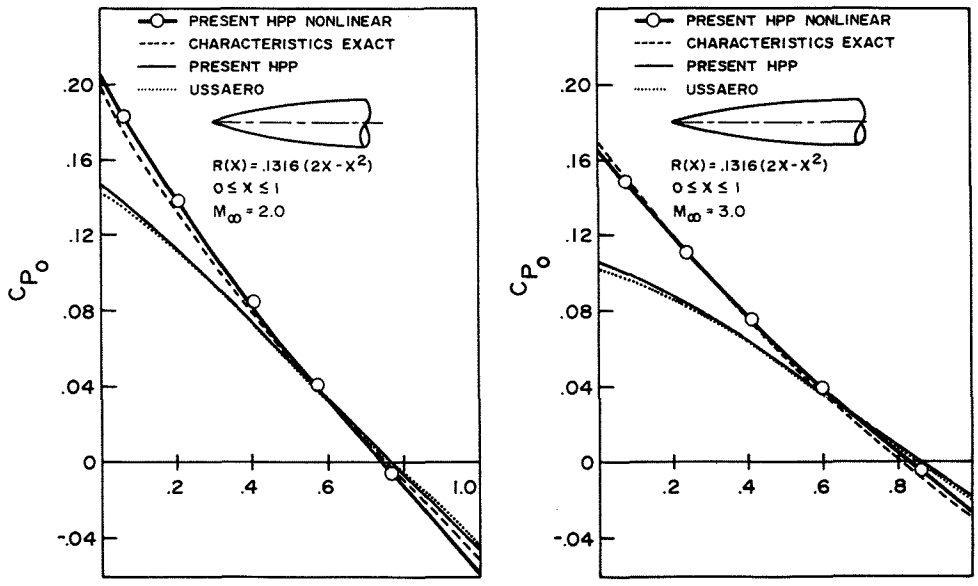

Fig. 3 Mean Flow Pressures for a Parabolic-Ogive at $M_\infty = 2.0$ and at Angle of Attack $\alpha_o = 0°$.

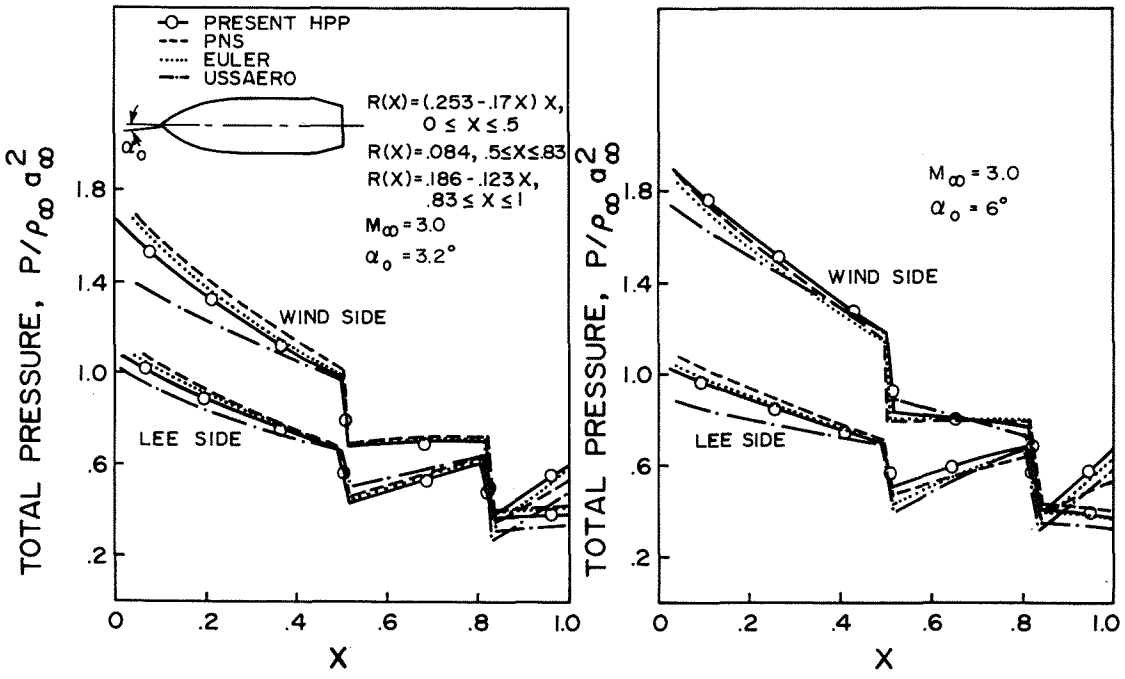

Fig. 4a, 4b Pressure Distribution of an Ogive-Cylinder-Boattail Body at $M_\infty = 3.0$ and Angle of Attack $\alpha_o = 3.2°$ and $6.3°$.

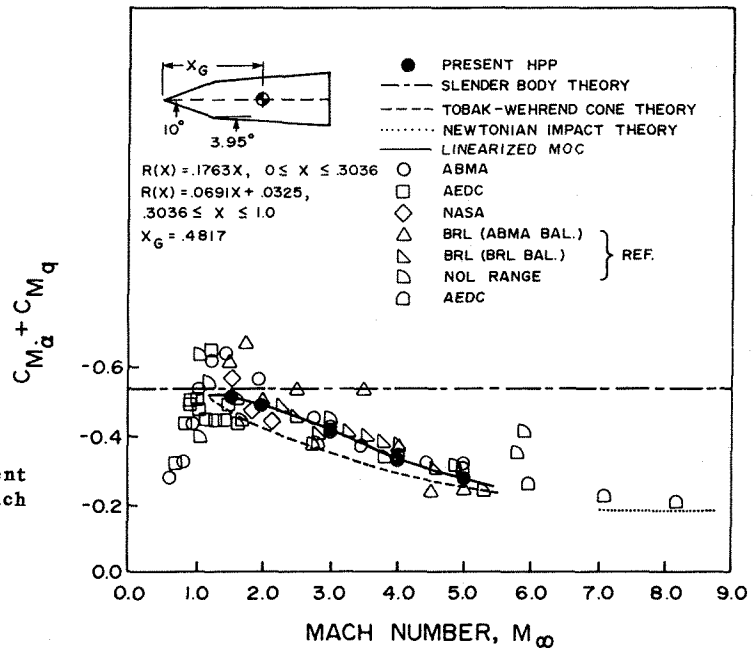

Fig. 6 Damping-in-Pitch Moment Coefficient for a Cone-Frustrum at Various Mach Numbers.

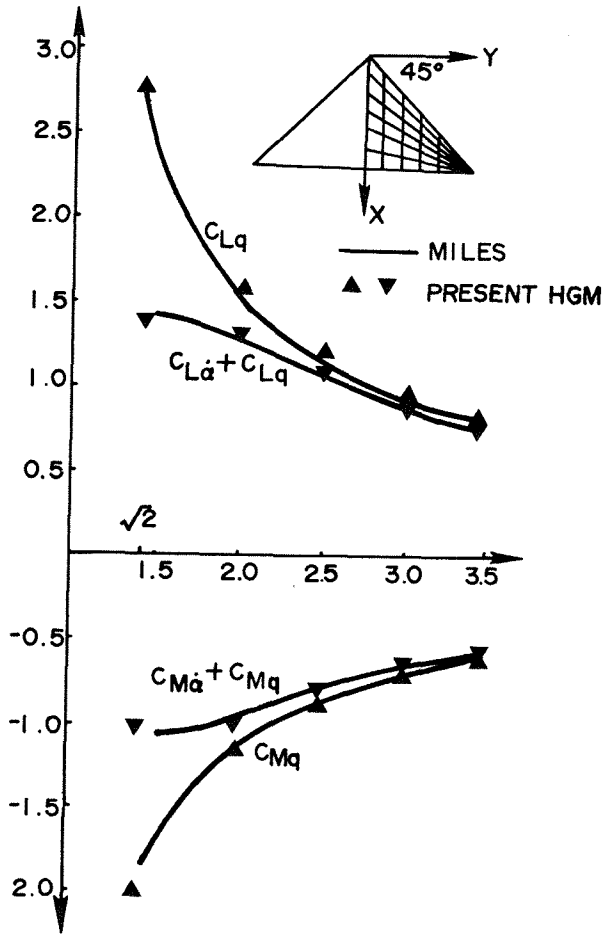

Fig. 5 Stability Derivatives of a 45° Delta Wing versus Various Mach Numbers.

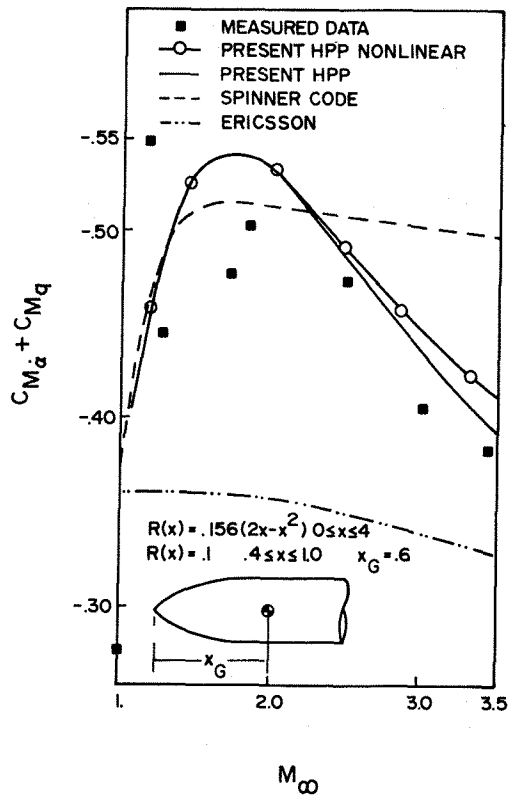

Fig. 7 Damping-in-Pitch Moment Coefficient for a Parabolic-Ogive-Cylinder at Various Mach Numbers.

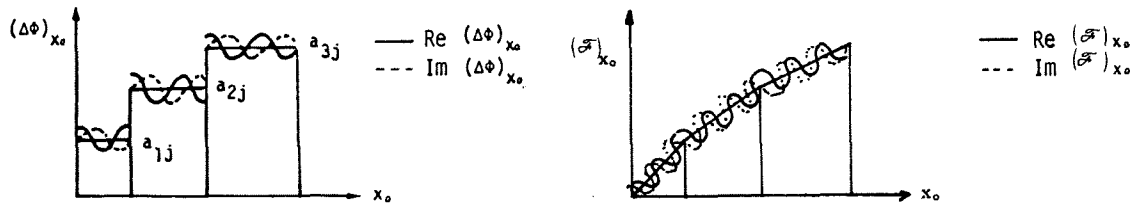

Fig. 8 Modeling of Dipole Strength.
(a) Harmonic Gradient Model (Wing)
(b) Harmonic Potential Panel Model (Body)

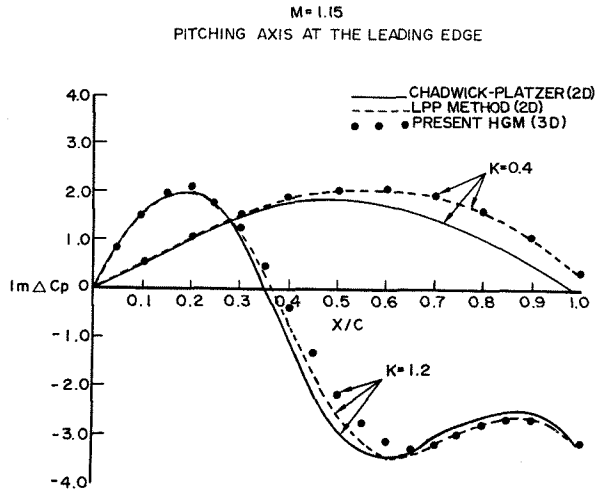

Fig. 9 Comparison of Unsteady Pressures with Various 2-D Methods at M_∞ = 1.15, k = .4 and k = 1.2. Pitching Axis at the Leading Edge.

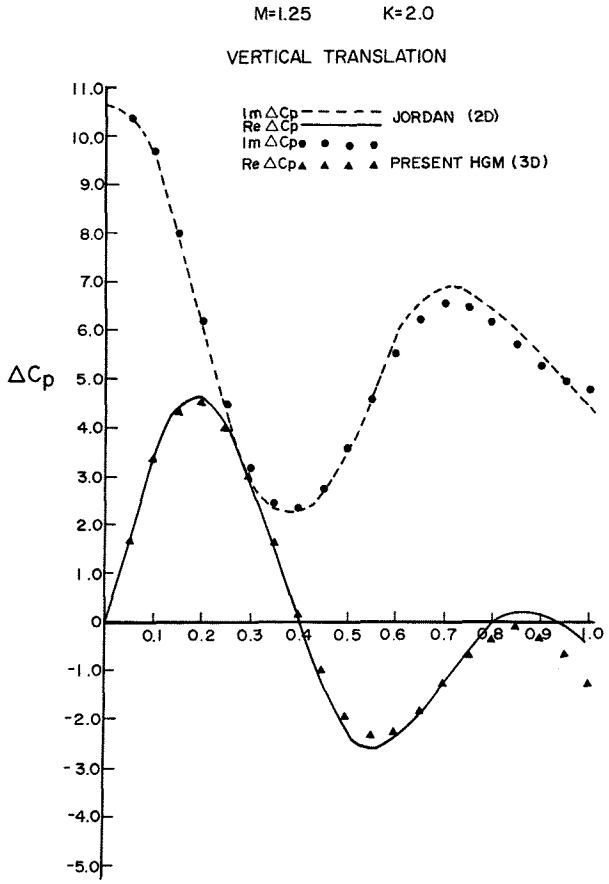

Fig. 10 Comparison of Unsteady Pressures Due to Plunging Motions with Jordan's 2D Method at M_∞ = 1.25 and k = 2.0.

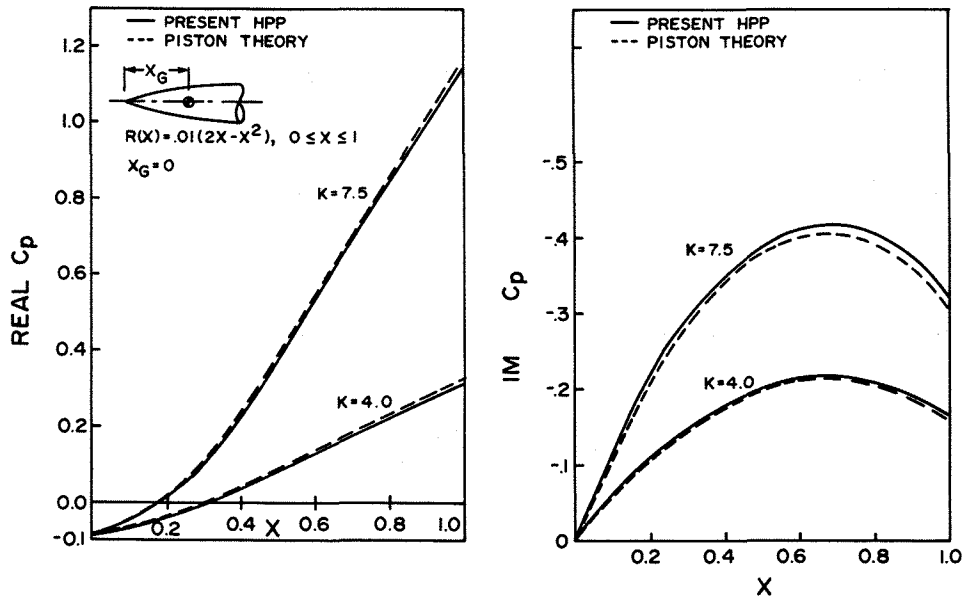

Fig. 11 In-phase and Out-of-phase Pressure Coefficients for a Parabolic-Ogive in Pitching Mode at M_∞ = 1.5 and High Reduced Frequencies.

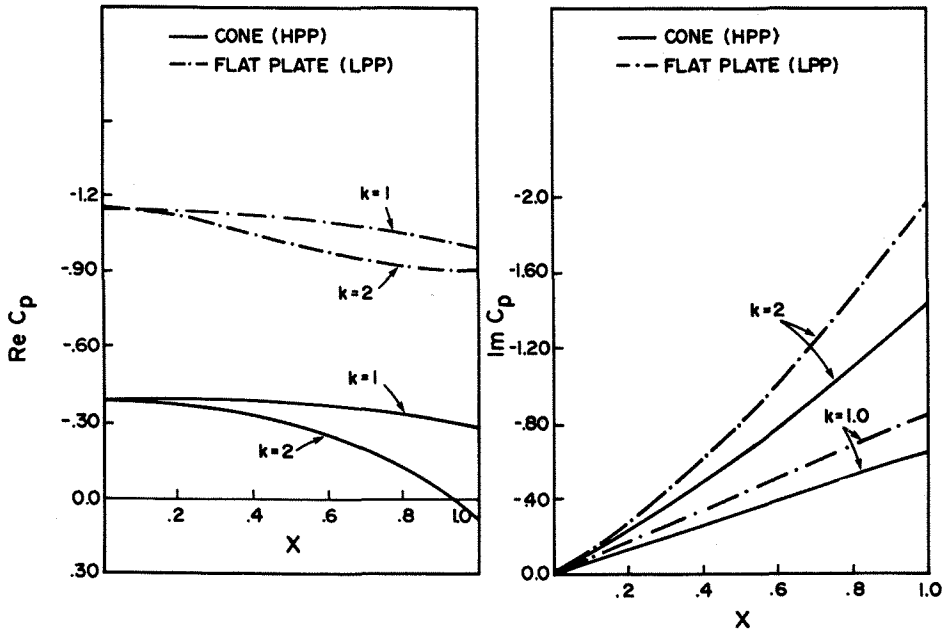

Fig. 12 Comparison of the In-phase and Out-of-phase Pressure Coefficients at M_∞ = 2.0 for a 5.7° Cone and a Flat Plate Pitching at the Apex.

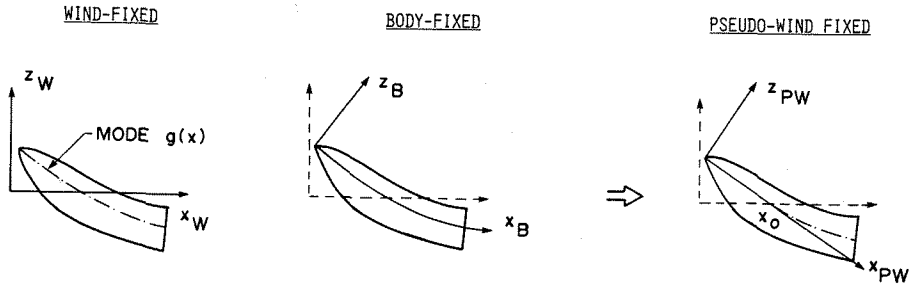

Fig. 13 Various Coordinate Systems for Oscillating Bodies.

Fig. 14 In-phase and Out-of-phase Pressure Coefficients for a Cone-Cylinder and a Parabolic-Ogive in First Bending Mode at $M_\infty = 2.5$ and Reduced Frequency k = 1.0.

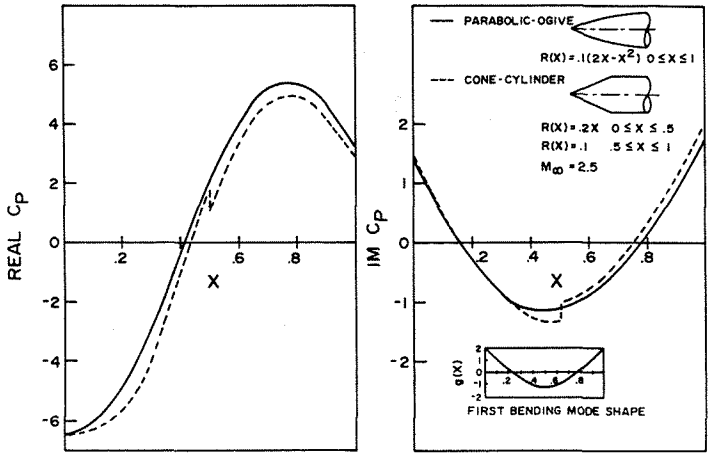

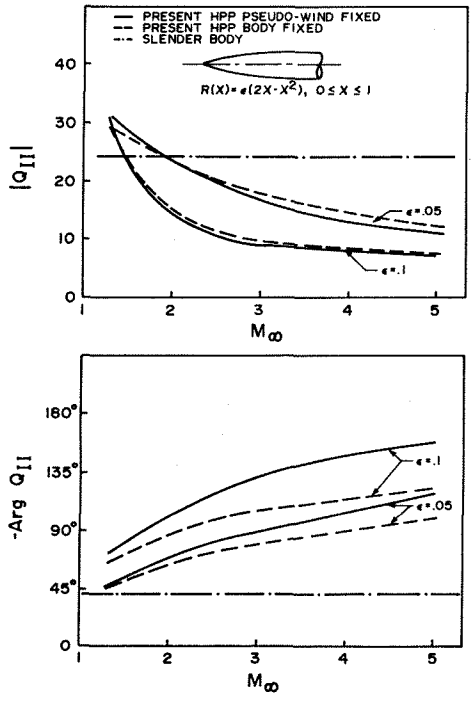

Fig. 15 Modulus and Argument of the Generalized Forces Versus Mach Number for a Parabolic Ogive in First Bending Mode at Reduced Frequency k = 2.0.

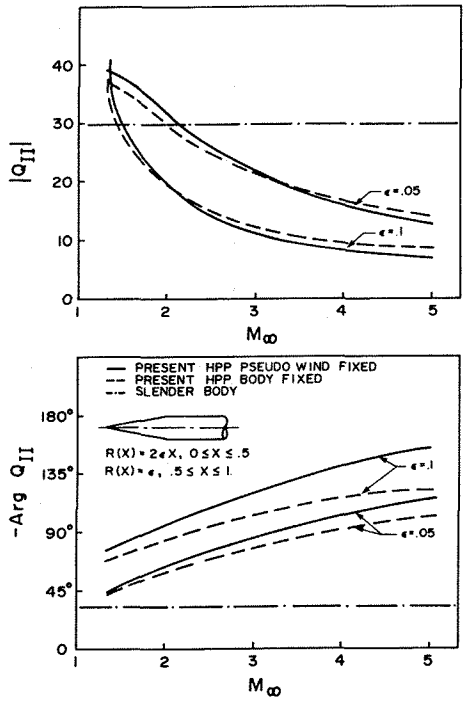

Fig. 16 Modulus and Argument of the Generalized Forces versus Mach Number for a Cone-Cylinder in First Bending Mode at Reduced Frequency k = 2.0.

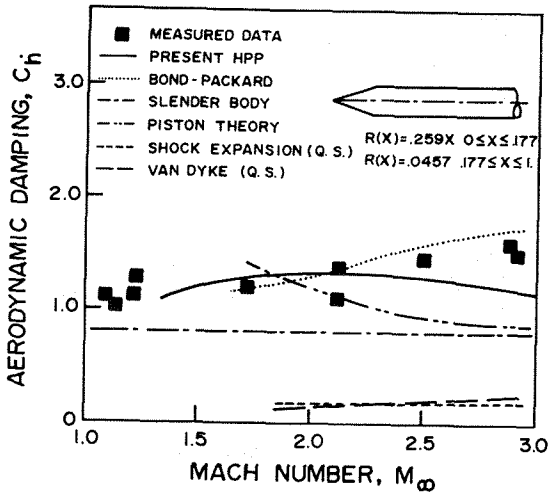

Fig. 17 Aerodynamic Damping Coefficients versus Mach Number for a Cone-Cylinder Vibrating in First Bending Mode (Data Taken from Ref. 23).

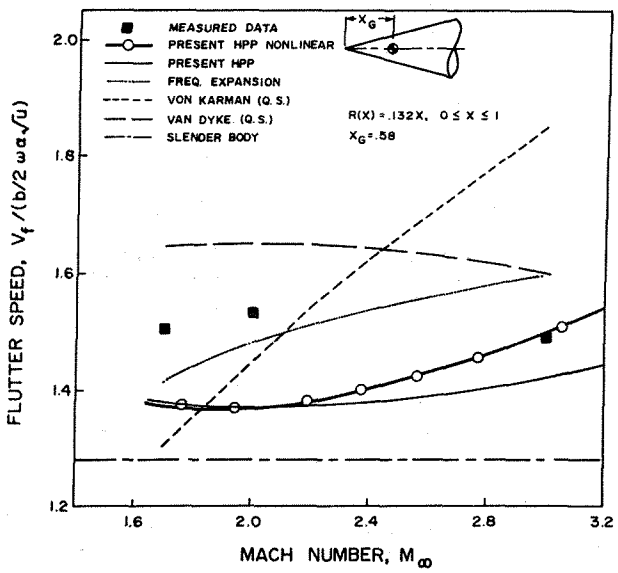

Fig. 19 Flutter Speed Boundaries versus Mach Number for a 7.5° Cone (Data Taken from Ref. 24).

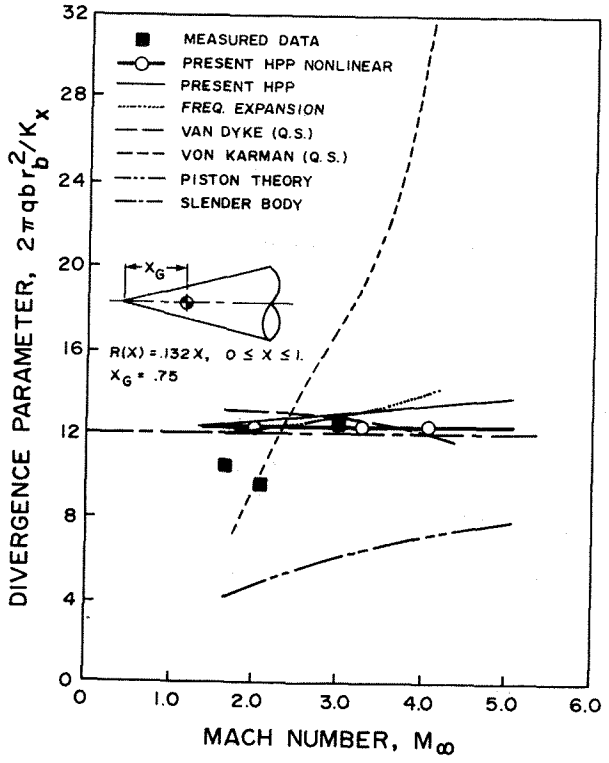

Fig. 18 Divergence Boundaries versus Mach Number for a 7.5° Cone (Data Taken from Ref. 24).

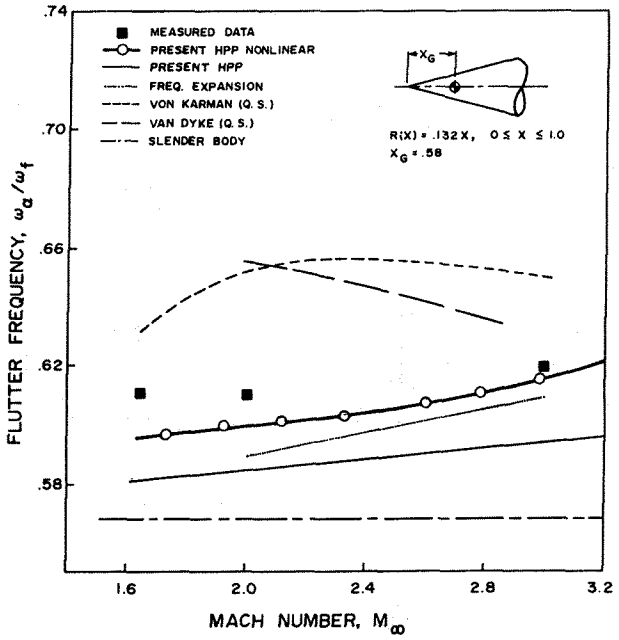

Fig. 20 Flutter Frequency Boundaries versus Mach Number for a 7.5° Cone (Data Taken from Ref. 24).

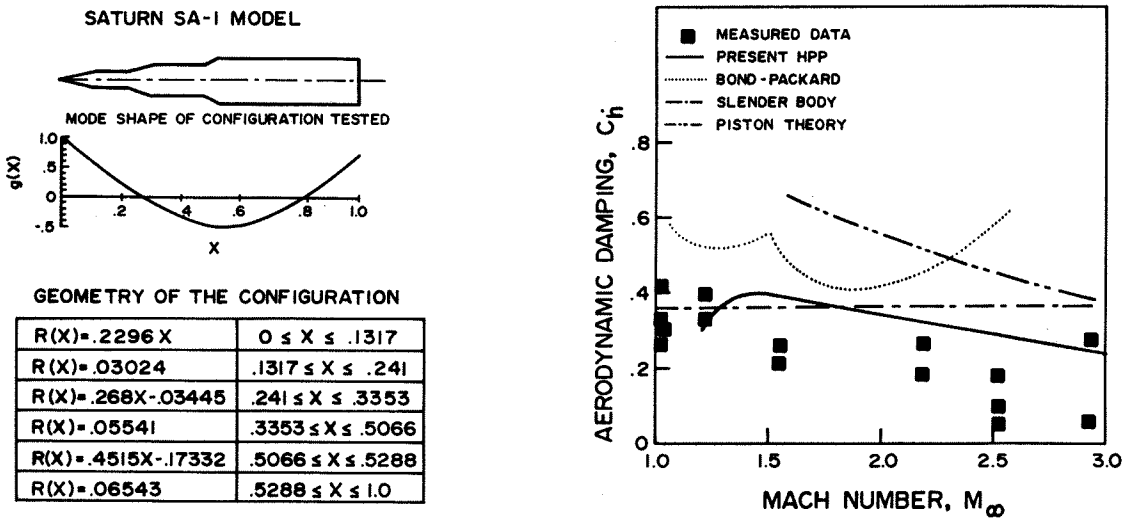

Fig. 21 Comparison of Computed and Experimental Aerodynamic Damping Coefficients versus Mach Number for a Saturn SA-1 Configuration Vibrating in First Bending Mode (Data Taken from Ref. 26).

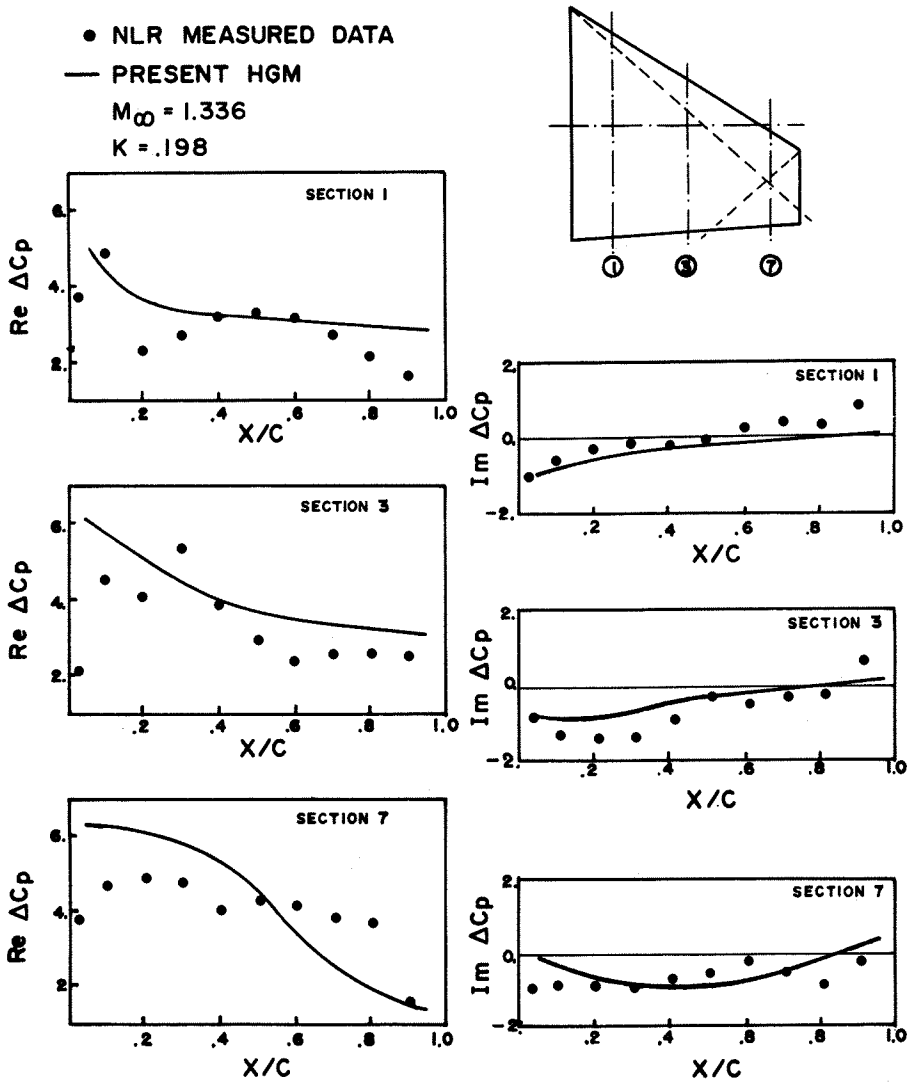

Fig. 22 Comparison of Computed Unsteady Pressure on a Northrop F-5 Wing with Experimental Data of NLR. Section 1 Y/B = 18%, Section 3 Y/B = 51.2%, Section 7 Y/B = 87.5%

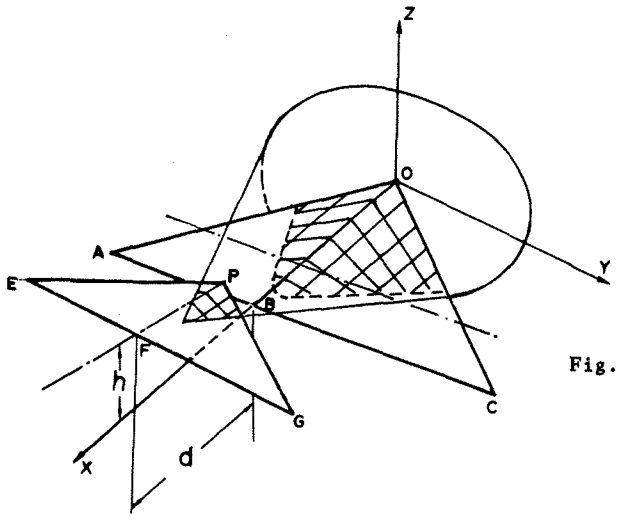

Fig. 23 Nonplanar Wing-Tail Configuration Showing Notations (OB = $2\sqrt{3}$, PF = $\sqrt{3}/2$, AC = 4 and EG = 2).

Table 1 Out-of-Phase Generalized Forces for Coplanar Tandem-Wing Interference, $M_\infty = 1.44$, $k = .01$.

	Case 1 d = 2.866 h = 0			/ Case 2 d = .866 h = 0		
Q''_{IJ}	HGM	Woodcock	Martin	/ HGM	Woodcock	Martin
11	3.073	2.951	2.99	3.160	2.88	3.06
12	1.439	1.473	1.43	0.348	0.20	0.37
13	0.489	0.469		0.489	0.477	
14	0.997	0.925		0.432	0.387	
21	0.345	0.326	0.32	0.259	0.110	0.21
22	4.102	4.142	4.40	1.104	0.970	1.70
23	1.055	1.016		0.490	0.483	
24	2.154	2.007		0.437	0.395	
31	0.151	0.149		0.238	0.07	
32	1.646	1.635		0.555	0.37	
33	0.489	0.469		0.489	0.477	
34	0.997	0.925		0.432	0.387	
41	0.324	0.321		0.238	0.09	
42	3.562	3.553		0.563	0.40	
43	1.055	1.016		0.490	0.483	
44	2.154	2.007		0.437	0.395	

Table 2 Out-of-Phase Generalized Forces for Nonplanar Tandem-Wing Interference, $M_\infty = 1.44$, $k = .01$.

Case 3 d = .866 h = .5 /			Case 4 d = .866 h = 1.0 /		Case 5 d = .866 h = 5.0	
Q''_{IJ}	HGM	Woodcock /	HGM	Woodcock /	HGM	Woodcock
11	3.161	2.954	3.065	3.028	3.412	3.282
12	0.264	0.170	0.269	0.141	0.225	0.214
13	0.489	0.477	0.489	0.477	0.489	0.477
14	0.432	0.387	0.432	0.387	0.432	0.387
21	0.272	0.171	0.164	0.240	0.512	0.499
22	1.026	0.934	1.018	0.896	0.977	0.971
23	0.490	0.483	0.490	0.483	0.490	0.483
24	0.437	0.395	0.437	0.395	0.437	0.395
31	0.239	0.148	0.142	0.222	0.489	0.477
32	0.471	0.343	0.476	0.315	0.432	0.387
33	0.489	0.477	0.489	0.477	0.489	0.477
34	0.432	0.387	0.432	0.387	0.432	0.387
41	0.250	0.155	0.112	0.224	0.490	0.483
42	0.485	0.358	0.478	0.319	0.437	0.395
43	0.490	0.483	0.490	0.483	0.490	0.483
44	0.437	0.395	0.437	0.395	0.437	0.395